

ONE DIMENSIONAL MIXED LUBRICATION REGIME MODEL FOR TEXTURED PISTON RINGS

Francisco J. Profito, fprofito@usp.br

Demetrio C. Zachariadis, dczachar@usp.br

Depto. de Engenharia Mecânica, EPUSP – Av. Prof. Mello Morais, 2231 – 05508-030 – São Paulo-SP

Eduardo Tomanik, eduardo.tomanik@br.mahle.com

MAHLE Metal Leve S.A. – Rodovia Anhanguera, km 49.7 – 13210-877 – Jundiá-SP

Abstract. *An one-dimensional model of the mixed lubrication regime for problems with general conditions of load, motion and geometry is presented. Such model derives from classical ones, such as the Reynolds equation related to the hydrodynamic phenomena and the Greenwood & Tripp formulation for the description of the asperity contact between rough surfaces. Cavitation of the lubricant was predicted adopting the complementary Swift-Steiber (or Reynolds) boundary conditions. As for the lubricant rheology, the viscosity-pressure dependence and viscosity-shear-thinning effects were considered as well.*

A computational program named VTL (Virtual Tribology Laboratory) was written for the simulation of the complete one-dimensional model. Comparisons between simulated and experimental results validate the proposed model and its numerical implementation. Next, the code was also used for the evaluation of the tribological behavior of textured piston rings.

Keywords: *Tribology, Lubrication, Roughness Topography, Piston Rings*

1. INTRODUCTION

The development of realistic mathematical models for the mixed lubrication regime has deserved attention in more recent years in order to enhance the prediction of the tribological performance of lubricated components during the engineering design stage. This arises from the ever increasing severity of the operational conditions of such components which leads to the growth of friction losses and wear.

In the mixed lubrication regime, the roughness of the surfaces plays an important role on both the hydrodynamic and contact phenomena. In the former, the micro-irregularities tend to disturb the lubricant flow whereas in the latter the micro-asperity contacts yield significant load carrying capacity as well as an increase in friction losses. Such effects are often neglected in conventional lubrication models, misleading the calculation of lubrication parameters for situations in which the lubricant film thickness has the same magnitude of the roughness heights.

Either deterministic or stochastic approaches may be employed in order to model the hydrodynamic and asperity contact effects in the mixed lubrication conditions. Pure deterministic formulations solve each of these effects in micro(roughness)-scale (Hu and Zhu, 2000). Consequently, due to the refined numerical meshes and hence higher computation time, simulations of practical lubrication problems are usually unfeasible. Mixed deterministic-stochastic formulations have been proposed in which the hydrodynamic and asperity contact are solved using stochastic and deterministic methodologies, respectively (Almqvist, 2006; Sahlin, 2008). The hydrodynamic problem is modeled using modified Reynolds equations that take into account the effect of the roughness on the lubricant flow by means of averaged 'flow factors' (Patir and Cheng, 1978; Fabricius, 2008). Finally, the use of pure stochastic formulations to model the influence of the roughness in the mixed lubrication regime (Salant et al., 2006; Thatte and Salant, 2009) is usually preferred due to the gain in computational robustness and efficiency. In this case, the hydrodynamic issue is described by adopting the above mentioned modified Reynolds equations ('flow factors') and the asperity contact according to an appropriated model that considers the statistical distribution of the asperities heights, e.g. Greenwood's formulations.

In this context, an one-dimensional model based on well established formulations is here proposed in order to mathematically model the mixed lubrication regime for sliding surfaces with general conditions of load, motion and geometry. The one-dimensional assumption is widely used in the scenery of piston ring simulations (Akalin and Newaz, 2001; Mufti et al., 2004; Jocsak et al., 2005). The development of the theoretical models is described and numerical results are validated by means of comparisons with experimental ones. This consolidated virtual tool was then used to investigate the tribological behavior of textured piston rings.

2. BRIEF DESCRIPTION OF LUBRICATION REGIMES

According to the motion, loading and lubricant viscosity conditions, lubricated systems undergo different lubrication regimes. In general three lubrication regimes are defined as shown in Fig. 1: boundary, mixed and full-hydrodynamic.

In the boundary lubrication regime almost all the load is supported by the inter-asperity/roughness contact and hence

no lubricant film is generated between the sliding surfaces. Actually, a tribological film of molecular dimensions is attached to the surfaces and the total external load is supported both by the direct contact between the asperities as well as by the interaction of the molecular film. In the mixed lubrication regime, a thin lubricant film is developed and the surfaces in contact are partially separated, i.e. part of the load is equilibrated by hydrodynamic forces and part by the asperity interactions. Finally, in the full-hydrodynamic regime, the lubricant oil film thickness is large enough to completely separate the lubricated surfaces (no asperity contact occurs).

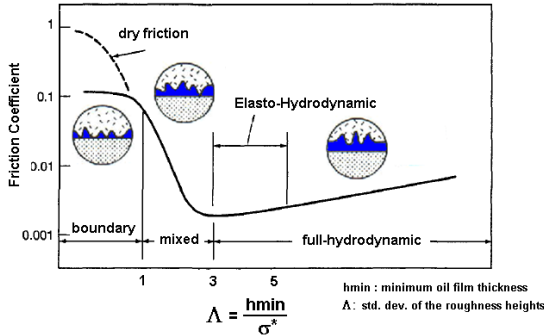


Figure 1. Typical Stribeck curve illustrating the lubrication regimes.

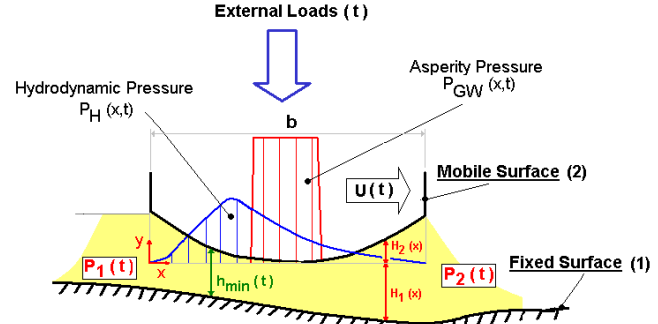


Figure 2. Overview of the tribosystem idealized for the mathematical model proposed in this work.

3. GOVERNING EQUATIONS OF THE MIXED LUBRICATION REGIME

As already mentioned, the asperity contact and hydrodynamic effects play an important role in the mixed lubrication regime. In the following, the models adopted in this work are described in details.

3.1. Modelling of the Hydrodynamic Forces

Reynolds Equation: The governing equation of the hydrodynamic pressure distribution in the fluid film is the Reynolds equation. Such equation is derived from the general Navier-Stokes equations after assuming the classical lubrication hypotheses, i.e. the surfaces are assumed smooth and the magnitude of the thickness of the fluid film is small compared to the other ones at the contact interface. For an isothermal and incompressible lubricant, the one-dimensional transient Reynolds equation is expressed as (Frene *et al.*, 1997):

$$\frac{\partial}{\partial x} \left[\frac{(H_2 - H_1)^3}{12\mu} \frac{\partial p_H}{\partial x} \right] = \left[\frac{U}{2} \frac{\partial [(H_2 - H_1)]}{\partial x} \right] + \left[-U \frac{\partial H_2}{\partial x} \right] + \left[\frac{\partial h_{min}}{\partial t} \right] \quad (1)$$

where p_H is the hydrodynamic pressure (Pa); μ the lubricant dynamic viscosity (Pa.s); U the slide velocity of the mobile surface (surface 1 is assumed fixed) (m/s); H_1, H_2 the geometry of the lubricant film (m) and h_{min} the minimum oil film thickness (m).

Throughout this work, it is assumed that only surface 2 (top) is moving. The effect of the roughness on the lubricant flow ('flow factors') was disregarded in the present model.

Lubricant Rheology: Temperature and pressure strongly influence the viscosity of lubricant oils. Furthermore, multigrade engine oils also exhibit shear-thinning effect due to the addition of friction modifier improvements. The viscosity model applied in this work takes temperature, pressure and shear rate influences into account by means of the Vogel, Barus and Cross correlations, respectively. Combining such rheology models, the following equation is obtained for the calculation of the viscosity correction (Stachowiak and Batchelor, 2005; Takata *et al.*, 2006):

$$\left\{ \mu(T, p_H, \dot{\gamma}) = a \cdot \exp \left\{ \underbrace{\frac{\alpha_B p_H}{\mu p_H}}_{\text{pressure effect}} + \underbrace{\frac{b}{T + c}}_{\text{temperature effect}} \right\} \cdot \underbrace{\left(\frac{1 + \frac{\mu_{\infty}}{\mu p_H} \left(\frac{\dot{\gamma}}{c_1 + c_2 T} \right)^m}{1 + \left(\frac{\dot{\gamma}}{c_1 + c_2 T} \right)^m} \right)}_{\text{shear-thinning effect}} \right. \quad (2)$$

$$\alpha_B = [0.6 + 0.965 \log_{10}(1000\mu_T)] \cdot 10^{-8}$$

where T is the lubricant temperature ($^{\circ}\text{C}$); $\dot{\gamma}$ the lubricant shear rate (s^{-1}); a, b, c the empirical constants of the Vogel equation and $c_1, c_2, m, \frac{\mu_{\infty}}{\mu p_H}$ the empirical constants of the Cross equation.

Boundary Conditions: The Reynolds equation (Eq. 1) is an elliptic partial differential equation of second order. In this sense, two boundary conditions are needed in order to completely define the hydrodynamic mathematical problem (see Fig. 2):

$$\begin{cases} p_H(0, t) = p_1(t) \\ p_H(b, t) = p_2(t) \end{cases} \quad (3)$$

where p_1, p_2 are the relative (inlet and outlet) boundary pressures (Pa) and b the length of the mobile surface (m).

Depending on the motion, geometry and boundary conditions of the lubricated system, cavitation takes place whenever the absolute local pressures fall below a minimum value (cavitation pressure). In such situations, the fluid film ruptures and a mixture of liquid (lubricant) and vapour/gas fills the cavitation zone. In the present work, the cavitation effects are taken in account in the Reynolds equations by means of the Swift-Steiber (or Reynolds) boundary conditions. These additional boundary conditions are defined as follows:

- The pressure gradients at the cavitation boundaries are zero. This condition ensures the mass-conserving only across the rupture boundaries:

$$\frac{\partial p}{\partial n} = 0 \quad - \quad \text{cavitation boundaries} \quad (4)$$

- The pressure within the cavitation regions are constant and equal to the vapour/gas-pressure of the lubricant (p_{cav}).

$$p \leftarrow p_{cav} = 0 \quad - \quad \text{within the cavitation regions} \quad (5)$$

The cavitation boundaries are unknown *a priori*. In this way, the solution of the hydrodynamic problem must be carried out employing iterative methods, like the ones based on the Finite Difference Scheme (FDS) with Successive Over-Relaxation (SOR) procedure (Venner and Lubrecht, 2000). In this case, the cavitation boundaries are automatically found setting to zero all pressures below p_{cav} .

3.2. Modelling Asperity Contact Forces

Greenwood & Tripp Formulation: The contact pressures arising from the interactions between the asperity summits of the rough surfaces are calculated using the Greenwood & Tripp model (Greenwood and Tripp, 1970):

$$p_{ASP}(x, t) = \begin{cases} \frac{16\pi\sqrt{2}}{15} E^* (\eta^2 \beta^{3/2} \sigma^{5/2}) F_{5/2}[\bar{h}(x, t)], & p_{ASP} \leq 3\sigma_{esc} \\ 3\sigma_{esc}, & p_{ASP} > 3\sigma_{esc} \end{cases} \quad (6)$$

where p_{ASP} is the asperity pressure (Pa); $\bar{h} = \frac{h-Z_s}{\sigma}$ the dimensionless separation distance between the mating surfaces (-); $Z_s = \sqrt{Z_{s1}^2 + Z_{s2}^2}$ the combined asperity summits mean height (m); $\sigma = \sqrt{\sigma_1^2 + \sigma_2^2}$ the combined asperity summits height standard deviation (m); $\beta = \sqrt{\frac{\beta_1^2 \beta_2^2}{\beta_1^2 + \beta_2^2}}$ the combined asperity summits mean radius (m); $\eta = \sqrt{\eta_1^2 + \eta_2^2}$ the combined asperity summits density (m⁻²); $E^* = \frac{E_1 E_2}{E_1(1-\nu_1^2) + E_2(1-\nu_2^2)}$ the composite elastic modulus (Pa); ν the Poisson's ratio (-) and σ_{esc} tensile strength of the softer surface (Pa). The subscripts denote each rough contact surface (see Fig. 2).

According to the Greenwood & Tripp model, it is assumed that both mating surfaces are covered by asperity summits paraboloidal in shape with constant radius β_i uniformly distributed with a density area η_i . The elastic deformation of each asperity is modelled based on the Hertzian contact theory and generalized throughout the contact interface according to the statistical description of the asperity heights. The function $F_{5/2}[\bar{h}(x, t)]$ in Eq. (6) represents the random distribution of the summits heights. Assuming a Gaussian distribution for the asperity heights, this function may be fitted by a sixth-order polynomial:

$$F_{5/2}(\bar{h}) = \frac{1}{\sqrt{2\pi}} \int_{\bar{h}}^{\infty} \left[(s - \bar{h})^2 e^{-\frac{s^2}{2}} \right] ds \approx \sum_{i=0}^6 a_i \bar{h}^i \quad , -3 < \bar{h} < 3 \quad (7)$$

$$a_0 = 6.153 \cdot 10^{-1}; a_1 = -1.085 \cdot 10^0; a_2 = 7.764 \cdot 10^{-1}; a_3 = -2.575 \cdot 10^{-1}$$

$$a_4 = 2.825 \cdot 10^{-2}; a_5 = 3.348 \cdot 10^{-3}; a_6 = -6.717 \cdot 10^{-4}$$

Furthermore, it is also assumed that interactions between the asperities will occur whenever the local dimensionless separation distance is less than three ($\bar{h} < 3$). In other words, asperity contact will be significant only if $h < (Z_s + 3\sigma)$.

Calculation of the Contact Parameters: As already exhibited in Eq. (6), the contact pressures are strongly dependent on the mechanical properties and roughness of the mating surfaces. The former are expressed by means of (E^*, σ_{esc}) whereas the latter from the contact parameters (Z_s, σ, β, η). Throughout this work, all contact parameters related to the surface topographies were calculated from actual roughness measurements employing the computational code MAHLE-SUMMITS (Tomanik *et al.*, 2003 and Tomanik, 2005). The software methodology assumes summits as the local maximum points above the surface (profile in one dimensional cases) mean plane (line) and the calculation of the

parameters (Z_s, σ, β, η) is strictly numerically done. Roughness filtering must be used in order to properly define the reference mean plane (line), especially when textured or honed topographies are considered (Profito *et al.*, 2010).

3.3. Equilibrium and Friction Forces

In the mixed lubrication regime, the external and inertial loads acting on the mobile surfaces are equilibrated by the hydrodynamic and asperity contact pressure fields (see item 3.1 and 3.2). As the mobile surface slides, a tangential friction force acts continually in the opposite direction of motion. This friction force is generated by the dissipative phenomena of the viscous flow and due to the interactions between the asperities. The free body diagram in figure 3 illustrates all forces acting on the mobile surface.

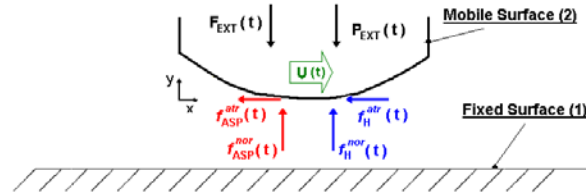


Figure 3. Free body diagram illustrating the forces acting on the mobile surface.

Equilibrium: Applying Newton's second law in the y direction for the mobile surface the following dynamic equation is obtained:

$$ma_y^G = f_H^{nor}(t) + f_{ASP}^{nor}(t) - F_{ext}(t) - bLP_{ext}(t) \quad (8)$$

where m is the mass of the mobile surface (kg); a_y^G the acceleration of the mobile surface in the y direction (m/s^2); $f_H^{nor}(t)$ the normal force (y direction) due to the hydrodynamic pressure field (N); $f_{ASP}^{nor}(t)$ the normal force (y direction) due to the asperity contact pressure field (N); $F_{ext}(t)$ the external force (N); $P_{ext}(t)$ the external pressure load (Pa); L the length of the mobile surface in the z direction (m).

Since the mass of the mobile surface is usually small, the inertia effects are neglected and Eq. (8) becomes:

$$\int_0^b [p_H(x, t) + p_{ASP}(x, t)] dx = \frac{F_{ext}(t)}{L} + bP_{ext}(t) \quad (9)$$

Friction Forces: The total friction force is a combination of the dissipative phenomena involving the hydrodynamic and asperity contact effects. The hydrodynamic friction is easily calculated from the Reynolds theory. For the asperity contact friction the simplest Coulomb's law is employed. Thus, the total friction force is evaluated as follows:

$$f_{TOTAL}^{fric}(t) = L \left\{ \underbrace{\int_0^b \left[\frac{(H_2 - H_1)}{2} \frac{\partial p_H}{\partial x} + \frac{\mu U}{(H_2 - H_1)} \right] dx}_{hydrodynamic \ friction} + \underbrace{\bar{\mu}_b \int_0^b [p_{ASP}(x, t)] dx}_{asperity \ contact \ friction} \right\} \quad (10)$$

where $\bar{\mu}_b$ is the boundary friction coefficient. The value of $\bar{\mu}_b$ must be known *a priori* in order to predict the mixed lubrication regime from the modelling presented in this work. The usual values of $\bar{\mu}_b$ are $0.1 < \bar{\mu}_b < 0.3$ (ASM Handbook, 1992), but more accurate values may be assessed from experimental friction tests.

Finally, the mixed friction coefficient can be calculated dividing the total friction force by the external loads acting on the mobile surface:

$$\bar{\mu}_{mixed}(t) = \frac{f_{TOTAL}^{fric}(t)}{F_{ext}(t) + bLP_{ext}(t)} \quad (11)$$

4. NUMERICAL ALGORITHM

The most important result of the solution of the one-dimensional model proposed in this work is the minimum oil film thickness (h_{min}) that yields the equilibrium (Eq. 9) at each time-step. Actually, the equilibrium is achieved by means of the hydrodynamic and asperity contact forces generated according to the separation distance of the surfaces.

At each time-step, the equilibrium condition (Eq. 9) is calculated iteratively using the Newton-Raphson method. In this sense, the adopted initial guess for the minimum oil film thickness is the converged one obtained on the previous step. The hydrodynamic pressure is calculated by the Reynolds equation (Eq. 1). The numerical solution of the Reynolds equation is based on the Finite Difference Scheme with the Successive Over-Relaxation method. Next, the contact pressure (Eq. 6) is evaluated solely in the positions where the local separation distance is smaller than ($Z_s +$

3σ). The influence of the temperature, hydrodynamic pressure and shear-thinning on oil viscosity is taken into account according to Eq. 2. Furthermore, for a reciprocating motion simulation, such as that discussed ahead, the complete cycle convergence is assumed whenever the maximum difference between all h_{min} 's of two consecutive cycles is below a given threshold. More details are given in Profito, 2010b.

All above mentioned numerical algorithm were implemented in a computational code named MAHLE-VTL (Virtual Tribology Laboratory). The source and the executable code are available in case of interest.

5. CODE VALIDATION

The experimental validation of the mathematical model proposed in this work was carried out considering the friction measurements taken during a reciprocating bench test published in Tomanik (2008). This bench test consists of two bodies sliding against each other by means of a reciprocating motion imposed by a crank-rod mechanism. In the specific situation considered for the code validation (Tomanik, 2008), piston ring samples were tested against two different bore finishes of combustion engines. Details of the test as well as the complete comparison between experimental and simulation results are presented ahead.

5.1. Test Description

The reciprocating bench test was conducted in a CETR UMT-2 equipment. Normal load is applied using a closed-loop servo mechanism, and normal load and friction forces are measured with strain-gages. A schematic illustration of the experimental setup is shown in Fig. 4.

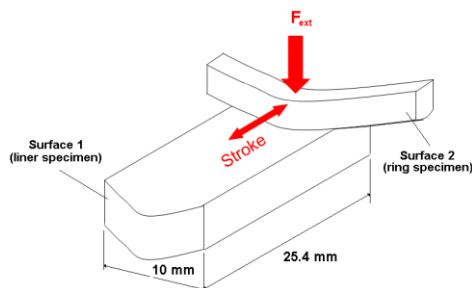


Figure 4. Schematic illustration of the reciprocating test.

The ring pieces were cut from production Heavy-Duty Diesel top rings, PVD CrN coated rings, 3 mm width. The bore finishes tested were samples of slide and plateau honing; representative roughness profiles are shown in Fig. 5.

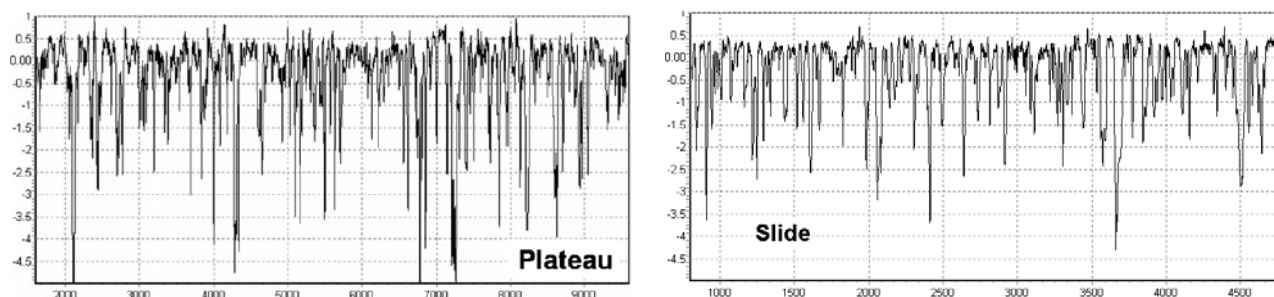


Figure 5. Representative roughness profiles of the bore finishes considered in this work.

For each bore finish, four replications were tested according to the following procedure:

- The liner specimens were flooded into 20 ml of SAE 30 Texaco Regal oil at ambient temperature ($\sim 30^{\circ}\text{C}$);
- Two load levels, 50 and 100 N, respectively, equivalent to nominal pressure of 0.14 and 0.28MPa;
- Speeds of the crank-rod mechanism: 50 N – (25, 50, 75, 100, 150, 250, 375 rpm);
 100 N – (50, 100, 150, 200, 300 rpm);
- Each speed/load condition was applied during 20 s; friction was acquired in the last ten seconds along the stroke. In order to check if break-in ("surfaces smoothing") during the friction tests was significant, two speed/load cases were repeated in the end. Effect of break-in along the sequence was considered negligible.

5.2. Test Simulation

The reciprocating test described above was reproduced by simulation for all speed/load conditions. The input data for simulation are summarized in table 1. The ring was assumed smooth and the contact parameters concerning the bore

topographies (slide and plateau honing finishes) were calculated from several roughness profiles like those illustrated in Fig 5. The face profile of the piston ring used in the simulation is shown in Fig. 6.

Table 1. Input data for the simulation of the reciprocating test used in order to validate the mathematical model proposed in this work.

General Test Parameters		Surface Parameters		
Lubricant	SAE30 at 30 °C	Ring Sample	Liner Samples	
Boundary Pressures	0 Pa	PVD "coating"	Slide Honing	Plateau Honing
External Force Load	50 N and 100 N	ν (-)	0.30	0.30
Speeds of the Crank-Rod Mechanism	25, 50, 75, 100, 150, 250 e 375 rpm	E (GPa)	250	120
Boundary Friction Coefficient ⁽¹⁾	0.12	σ_{esc} (MPa)	500	250
Stroke Length	10 mm	Z_s (μm)		0.33
Rod Length	56 mm	σ (μm)		0.25
		β (μm)		13.1
		η (m^2)		3.5E10
				2.8E10

(1): determined from the experimental results

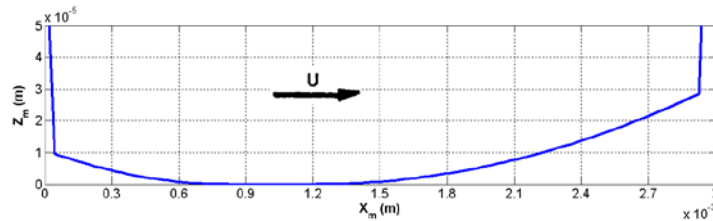


Figure 6. Face profile of the piston ring used in the simulation for the validation of the mathematical model proposed in this work.

At each speed/load condition, the sliding velocity of the mobile surface (ring specimen) changes along the stroke due to the reciprocating motion (maximum velocities at the mid-stroke and minimum at the reversal points). Likewise, all the calculated results, i.e. minimum oil film thickness, mixed friction coefficients, hydrodynamic and asperity contact pressure etc, will vary along the stroke. Figure 7 illustrates these results for the condition 375 rpm / 50 N (slide honing case).

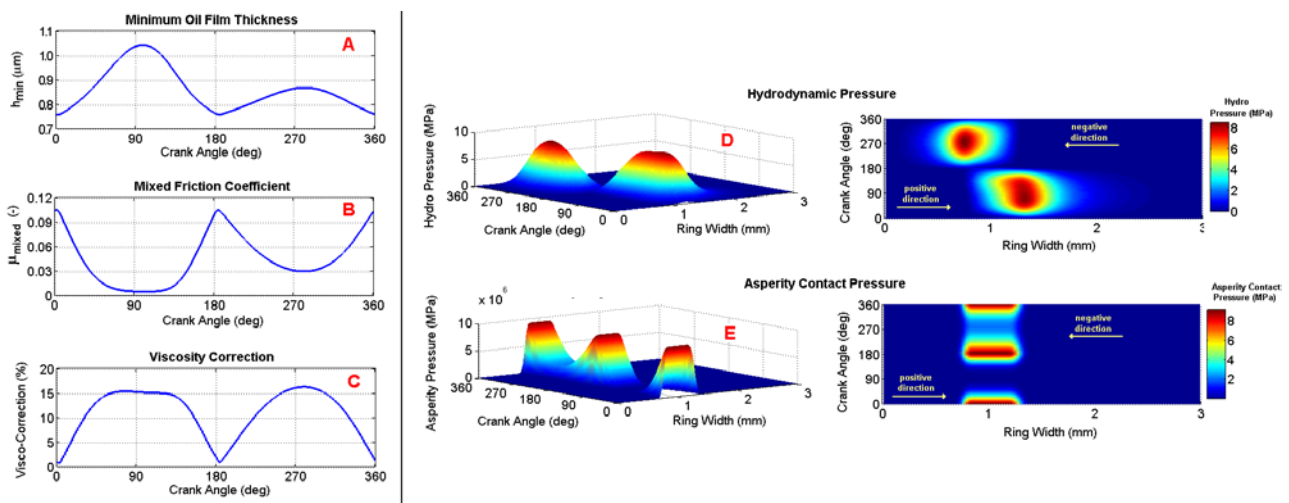


Figure 7. Complete simulation results for the condition 375 rpm / 50 N (slide honing case).

Due to the ring non-symmetrical face running profile (see Fig. 6), the results related to the forward and backward sliding are slightly different. At the mid-stroke (crank angles $\sim 90^\circ$ and $\sim 270^\circ$) the sliding velocities are higher and hence increase the hydrodynamic effects (higher hydrodynamic pressures, see Fig. 7-D). In this situation, the minimum oil film thickness are larger (see Fig. 7-A) yielding the reduction of the asperity interactions (lower asperity contact pressures, see Fig. 7-E). As a consequence, the mixed friction coefficients at the mid-stroke are smaller than in the other positions along the reciprocating motion (see Fig. 7-B). The contrary happens close to the reversal points (crank angles $\sim 0^\circ$, $\sim 180^\circ$ and $\sim 360^\circ$).

5.3. Comparison Between Experimental and Simulation Results

The experimental and simulation results of the reciprocating friction test are compared in terms of the cycle averaged friction coefficients, i.e. the mean value of the friction coefficients along a complete reciprocating cycle. Such quantity gives a thorough measure of the friction losses for each speed/load conditions and is defined as follows:

$$\bar{\mu}_{cycle\ avg.} = \frac{1}{360} \int_0^{360} \bar{\mu}_{mixed}(\theta) \cdot d\theta \quad (12)$$

where θ is the crank angle.

The global results are summarized by means of a Stribeck-like curve where the cycle averaged friction coefficients are plotted as a function of the speed/load ratio. For the sake of simplicity, only friction coefficients in the positive direction (forward sliding) and for 50 N cases are shown. The 100 N cases showed similar ranking. Figure 8 compares the experimental and simulation results of the reciprocating test discussed so far.

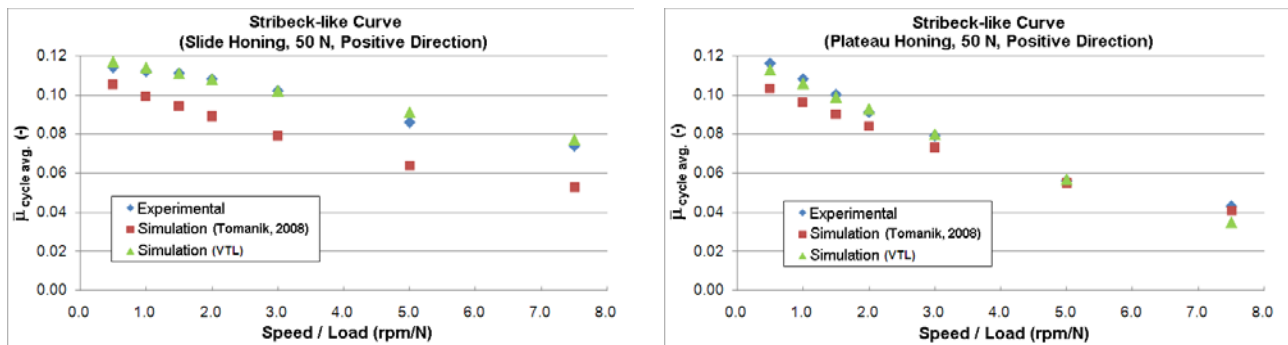


Figure 8. Comparison between experimental and simulation results of the reciprocating test.

According to the plots in Fig. 8, as the crank-rod speed increases the friction coefficients tend to diminish. From the classical Stribeck's theory, such behaviour indicates that the lubrication regime is mixed. One notes that the original Stribeck curve was proposed for steady-state lubrication conditions instead of reciprocating ones, and the abscissa of the original curve is built regarding the linear velocities (m/s). Although the velocity values in the Stribeck-like curve used in this work are calculated employing the crank-rod speeds (rpm), the physical kinematic trends are kept once the magnitude of the linear velocities increases together with the crank-rod speed.

Three kinds of results are plotted in Fig. 8: experimental (blue diamonds); literature (Tomanik, 2008) (red squares); calculated using the mathematical model and computational implementation described in this work (green triangles). The numerical results published in Tomanik (2008) are based on a mathematical model of friction in piston rings developed by MIT's (Massachusetts Institute of Technology) researchers.

Finally, it is possible to conclude that the simulated results obtained with the one-dimensional model described in this work yield a good correlation with the experimental ones.

6. SIMULATIONS WITH TEXTURED PROFILES

In order to explore the use of surface texturing for friction reduction in piston rings assemblies, some numerical simulations were carried out employing the mathematical model previously described. Unlike the barrel shape profile used in the simulation of the reciprocating test (see Fig. 6), now the running face of the piston rings was assumed flat with micro-grooves full and partially distributed (see Fig. 9 and table 2). The adoption of grooves is coherent with the one-dimensional approach employed throughout this work.

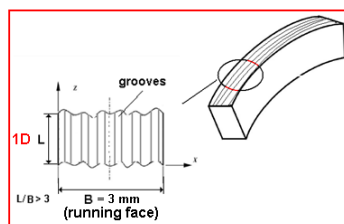


Figure 9. Illustration of the micro-grooves machined to the flat piston rings.

6.1. Dimensions of the Grooves

The dimensions of the micro-grooves considered in the next simulations are listed in table 2. Such dimensions were extracted from the literature (Ryk *et al.*, 2005; Ryk and Etsion, 2006; Etsion and Sher, 2009) and are the typical ones

suggested for flat piston rings with micro-dimples texturing.

Table 2. Dimensions of the micro-grooves used in the simulations

Dimensions (μm)	Full Texturing	Partial Texturing
Diameter: 100 Depth: 10 Pitch: 150		
Diameter: 100 Depth: 10 Pitch: 250		
Diameter: 100 Depth: 10 Pitch: 450		

6.2 Results for Steady-State Simulations

In order to understand the physics of the lubrication when micro-grooves are taken into account on the contact interface, some steady-state simulations were performed. For all situations, the velocity of the mobile surface (textured) was assumed 1 m/s and the minimum oil film thickness was fixed as 1 μm . The latter assumption was chosen instead of using external loads for iteratively calculating the minimum oil film thickness, in order to compare the performance of the different texturing variants by means of the values of the hydrodynamic load carrying capacity. All other parameters for simulation are the same ones listed in table 1 for the slide honing case. Table 3 summarizes the values of the hydrodynamic load carrying capacity calculated for each texturing variants.

Table 3. Hydrodynamic load carrying capacity calculated for the flat textured profiles at the steady-state condition.

Diameter (μm)	Depth (μm)	Pitch (μm)	Hydrodynamic Capacity (N)	
			Full Texturing	Partial Texturing
100	10	150	48.5	216.8
100	10	250	54.9	131.3
100	10	450	50.0	84.4

The highest load carrying capacity was obtained with partial texturing, especially for the variant with smallest grooves pitch, i.e. highest groove density (see table 3). Figure 10 illustrates the hydrodynamic and asperity contact pressures fields for this texturing variant (diameter: 100 μm ; depth: 10 μm ; pitch: 150 μm ; full and partial texturing). In this figure, the lubricant flow is from right to left (see the velocity direction).

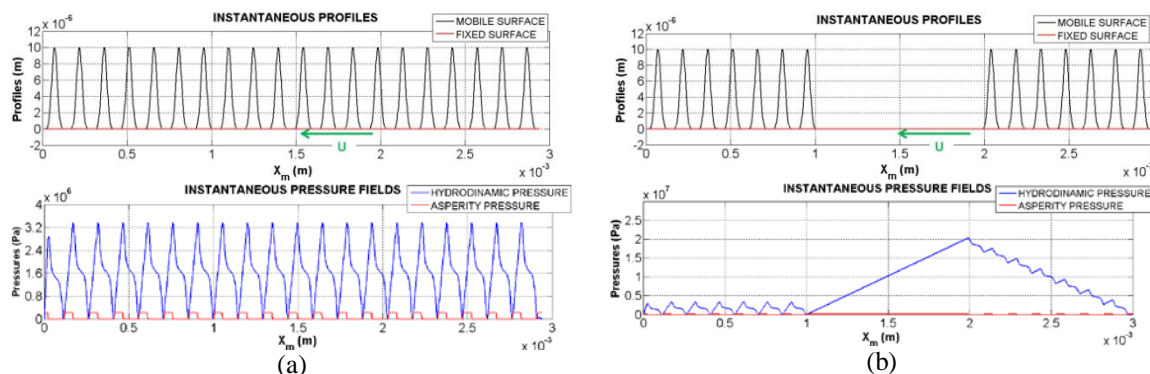


Figure 10. Hydrodynamic and asperity contact pressures for the texturing variant (diameter: 100 μm ; depth: 10 μm ; pitch: 150 μm). (a) Full texturing. (b) Partial texturing.

The individual effect of the micro-grooves is determinant for full texturing configurations (see Fig. 10a). In these situations, hydrodynamic load capacity is generated due to the cavitation phenomenon which occurs around the divergent portion of each groove. The maximum hydrodynamic pressures are observed at the convergent regions where the "physical wedge" effect takes place (micro-bearing effect). Furthermore, it is interesting to point out the generation of hydrodynamic pressures even in the flat portions between each micro-groove. Such effect occurs due to the non-zero

pressures observed upstream each groove, making these intermediated flat regions behave like micro-hydrostatic bearings with linear pressure distribution.

For partial texturing, the collective effect of the micro-grooves is observed by the "accumulation" of hydrodynamic pressure at the initial textured portion on the right side of the flat profile (see Fig. 10b). This "accumulation" of pressure is generated due to a mechanism similar to the inlet roughness concept (Tonder, 2001) in which the partial texturing creates an "effective clearance" reduction in the sliding direction. In other words, the mean difference of the geometry between the textured and non-textured portions creates an "equivalent Rayleigh-step" (see Fig. 11) that generates significant hydrodynamic pressures. Such collective effect tends to produce more load carrying capacity than the individual effect described for full texturing (Brizmer *et al.*, 2003). In this sense, partial texturing is always recommended for flat piston rings regardless of the position of the textured portions (Ryk *et al.*, 2005; Ryk and Etsion, 2006; Etsion and Sher, 2009).

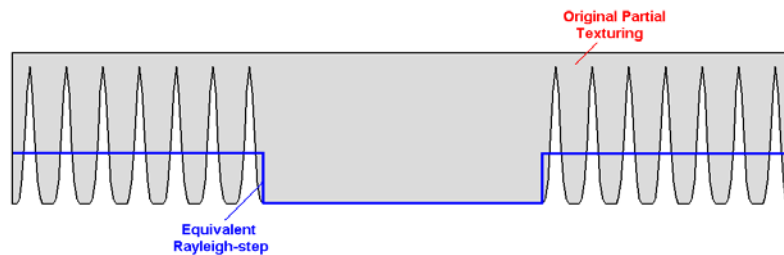


Figure 11. Scheme of the "Equivalent Rayleigh-step" created with partial texturing.

Further results concerning the simulation of the reciprocating test with textured surfaces can be found in Profito (2010b) and will be addressed in future publications.

7. CONCLUSIONS

An one-dimensional model of the mixed lubrication regime was proposed based on classical formulations in order to describe the hydrodynamic and asperity contact phenomena. The former was done employing the classical transient Reynolds equation whereas the latter by the stochastic Greenwood & Tripp theory. The cavitation of the lubricant was considered adopting the Swift-Steiber (or Reynolds) complementary boundary conditions. Furthermore, the lubricant viscosity corrections due to the temperature, hydrodynamic pressure and shear-thinning effects were also taken in account by means of the Vogel, Barus and Cross correlations, respectively.

A computational program named MAHLE-VTL (Virtual Tribology Laboratory) was developed in order to numerically solve the proposed mathematical model. The code was validated by means of comparisons between calculated and experimental results concerned with two different bore topographies, i.e. slide and plateau honing, of internal combustion engines. The correlation between experimental and numerical results was excellent. The code performs simulations of lubrication problems with general conditions of load, motion and geometry. The program is an open source code and a GUI (Graphical User Interface) version will be released in the near future.

In order to investigate the potential use of surface texturing for friction reduction, numerical simulations were carried out considering flat piston rings fully and partially textured with micro-grooves. Confirming previous results (Brizmer *et al.*, 2003), partial texturing yielded higher hydrodynamic load carrying capacity than full texturing. One notices that due to the limitations of the mathematical model proposed in this work, a deeper analysis must be developed in order to enhance the prediction of the hydrodynamic effects for situations involving more complex lubricated textured surfaces, e.g. consideration of bidimensional flow effects (2D Reynolds equation), enforcement of mass-conservation throughout the cavitation boundaries (JFO cavitation model), inclusion of inertia effects and the influence of the roughness on the lubricant flow ('flow factors').

Despite of the limitations of the one dimensional model proposed in this work, it may be employed as a virtual tool in order to analyze the following effects that influence the mixed lubrication regime:

- different surface topographies (Greenwood's contact parameters);
- different lubricants/viscosities;
- effect of viscosity-temperature-pressure-shear corrections;
- different contact geometries without discontinuities (micro-grooves);
- misalignment of specimens in tribology bench tests;
- good description of the micro-bearing mechanism that generates hydrodynamic load carrying capacity between parallel textured surfaces, e.g. micro-grooves.

8. ACKNOWLEDGEMENTS

This work was sponsored by MAHLE Metal Leve S.A.

9. REFERENCES

- Akalin, O., Newaz, G.M., 2001. "Piston Ring –Cylinder Bore Friction Modeling in Mixed Lubrication Regime: Part I – Analytical Results". Transactions of ASME – Journal of Tribology, Vol. 123, No. 1, pp. 211-218.
- Almqvist, A., 2006. "On the Effects of Surface Roughness in Lubrication". PhD thesis, Lulea University of Technology – Lulea, Sweden.
- ASM Handbook – Vol. 18: Friction, Lubrication and Wear Technology. 1992.
- Brizmer, V., Kligerman, Y., Etsion, I., 2003. "A Laser Surface Textured Parallel Thrust Bearing". Tribology Transactions, Vol. 46, No. 3, pp. 397-403.
- Etsion, I., Sher, E., 2009. "Improving Fuel Efficiency with Laser Surface Textured Piston Rings". Tribology International, Vol. 42, No. 4, pp. 542-547.
- Fabricius, J., 2008. "Homogenization Theory with Applications in Tribology". PhD thesis, Lulea University of Technology – Lulea, Sweden.
- Frene, J., Nicolas, D., Berthe, D., Godet, M., 1997. "Hydrodynamic Lubrication: Bearings and Thrust Bearings (Tribology Series, 33)". Ed. Elsevier Science, Amsterdam, The Netherlands, 499 p.
- Greenwood, J. A., Tripp, J. H., 1970. "The Contact of Two Nominally Flat Rough Surfaces", Proceedings of the Institution of Mechanical Engineers, Vol. 185, No. 48, pp. 625-633.
- Hu, Y.-Z., Zhu, D., 2000. "A Full Numerical Solution to the Mixed Lubrication in Point Contacts", Transactions of ASME – Journal of Tribology, Vol. 122, No. 1, pp. 1-9.
- Jocsak, J., Li, Y., Tian, T., Wong, V.W., 2005. "Analyzing the Effects of Three-Dimensional Cylinder Bore Liner Surface Texture on Ring-Pack Performance with Focus on Honing Grooves Cross-Hatch Angle". Proceedings of ASME Internal Combustion Engine Division Fall Technical Conference – ICEF2005-1333.
- Mufti, R.A., Priest, M., Chittenden, R.J., 2004. "Experimental and Theoretical Study of Instantaneous Piston Assembly Friction in a Gasoline Engine". Proceedings of International Joint Tribology Conference – TRIB2004-64199.
- Patir, N., Cheng, H.S., 1978. "An Average Flow Model for Determining Effects of Three-Dimensional Roughness on Partial Hydrodynamic Lubrication", Journal of Lubrication Technology, Vol. 100, No. 1, pp. 12-17.
- Profito, F., Tomanik, E., Zachariadis, D.C., 2010. "An Improved Surface Characterization of Textured Surfaces on Mixed Lubrication Regimes". SAE Technical Paper Series, SAE2010-01-1525.
- Profito, F., 2010. "Modelagem Unidimensional do Regime Misto de Lubrificação Aplicada a Superfícies Texturizadas". Dissertação de Mestrado, Escola Politécnica da Universidade de São Paulo.
- Qiu, Y., Khonsari, M. M., 2009. "On the Prediction of Cavitation in Dimples Using a Mass-Conservative Algorithm". Transactions of the ASME – Journal of Tribology, Vol. 131, No. 4, pp. 041702(11 pages).
- Ryk, G., Kligerman, Y., Etsion, I., Shinkarenko, A., 2005. "Experimental Investigation of Partial Laser Surface Texturing for Piston Rings Friction Reduction". Tribology Transactions, Vol. 48, No. 4, pp. 583-588.
- Ryk, G., Etsion, I., 2006. "Testing Piston Rings with Partial Laser Surface Texturing for Friction Reduction". Wear, Vol. 261, pp. 792-796.
- Stachowiak, G. W., Batchelor, A. W., 2005. "Engineering Tribology". Third edition. Ed. Elsevier Butterworth-Heinemann, Oxford, UK, 831 p.
- Sahlin, F., 2008. "Lubrication, Contact Mechanics and Leakage between Rough Surfaces". PhD thesis, Lulea University of Technology – Lulea, Sweden.
- Salant, R.F., Maser, N., Yang, B., 2006. "Numerical Model of a Reciprocating Hydraulic Rod Seal". Proceedings of International Joint Tribology Conference – IJTC2006-12075.
- Takata, R., Li, Y., Wong, V. W., 2006. "Effects of Lubricant Viscosity on Ring/Liner Friction in Advanced Reciprocating Engine Systems". ASME-ICEF 2006 Fall Technical Conference, ICEF2006-1526.
- Thatte, A., Salant, R.F., 2009. "Elastohydrodynamic Analysis of an Elastomeric Hydraulic Rod Seal During Fully Transient Operation". Transactions of ASME – Journal of Tribology, Vol. 131, No. 3, 031501 (11 pages).
- Tomanik, E., Chacon, H., Teixeira, G., 2003. "A Simple Numerical Procedure to Calculate the Input Data of Greenwood-Williamson Model of Asperity Contact for Actual Engineering Surfaces". Leeds-Lyon Symposium on Tribology: Tribological Research and Design for Engineering Systems, Tribology Series, Vol. 41, pp. 205-216.
- Tomanik, E., 2005. "Modelling of the Asperity Contact Area on Actual 3D Surfaces". SAE Technical Paper Series, SAE2005-01-1864.
- Tomanik, E., 2008. "Friction and Wear Bench Tests of Different Engine Liner Surface Finishes". Tribology International, Vol. 41, pp. 1032-1038.
- Tonder, K., 2001. "Inlet Roughness Tribodevices: Dynamic Coefficients and Leakage. Tribology International, Vol. 34, pp. 847-852.
- Venner, C. H., Lubrecht, A. A., 2000. "Multilevel Methods in Lubrication (Tribology Series, 37)", Ed. Elsevier Science, The Netherlands, 401 p.

10. RESPONSIBILITY NOTICE

The authors are the only responsible for the printed material included in this paper.